based on Method 3 is unconditionally stable, and the programs based on Methods 1 and 2 are not always stable.

4. CONCLUSION

In this article three methods with regard to the PEC condition implementation of the ADI-FDTD scheme are discussed. It is found that the method in which the PEC condition is directly incorporated within the tridiagonal matrix system is most accurate. Although it is complicated, this method is efficient, stable, and more suitable to ADI-FDTD scheme with large CFLN. The validity of this algorithm is confirmed through numerical examples.

REFERENCES

1. T. Namiki, A new FDTD algorithm based on alternating-direction implicit method, IEEE Trans Microwave Theory Tech 47 (1999), 2003–2007.
2. F. Zheng, Z. Chen, and J. Zhang, A finite-difference time-domain method without the courant stability conditions, IEEE Microwave Guided Wave Lett 9 (1999), 441–443.
3. T. Namiki, 3-D ADI-FDTD method-unconditionally stable time-domain algorithm for solving full vector Maxwell's equations, IEEE Trans Microwave Theory Tech 48 (2000), 1743–1748.
4. T.W. Lee and S. C. Hagness, Wave source conditions for the unconditionally stable ADI-FDTD method, Proc IEEE Antennas Propag Soc Int Symp 4 (2001), 142–145.
5. A. Zhao, Two special notes on the implementation of the unconditionally stable ADI-FDTD method, Microwave Opt Technol Lett, 33 (2002), 273–277.
6. S.G. García, A.R. Bretones, R.G. Martín, and S.C. Hagness, Accurate implementation of current sources in the ADI-FDTD Scheme, IEEE Antennas Wireless Propag Lett 3 (2004), 141–144.
7. S. Wang, On the current source implementation for the ADI-FDTD method, IEEE Microwave Wireless Compon Lett 14 (2004), 5131–515.
8. B. Donderici and F.L. Teixeira, Symmetric source implementation for the ADI-FDTD method, IEEE Trans Antennas Propag 53 (2005), 1562–15659.

BAND-STOP FILTER BASED ON A SUBSTRATE EMBEDDED WITH METAMATERIALS

Soon-Cheol Kong, Zachary M. Thomas, Xudong Chen, Bae-Ian Wu, Tomasz M. Grzegorczyk, and Jin Au Kong
Massachusetts Institute of Technology, 77 Massachusetts Avenue, Room 26–305, Cambridge, MA 02139-4307

Received 12 July 2006

ABSTRACT: *The effects of embedding SRR into a substrate of microstrip line are investigated, in particular in transmission. The simulation and experimental results show band-stop property of the device. Also, reduced radiation loss and device volume are achieved by applying the image theory from a symmetric SRR.* © 2007 Wiley Periodicals, Inc.
Microwave Opt Technol Lett 49: 530–534, 2007; Published online in Wiley InterScience (www.interscience.wiley.com). DOI 10.1002/mop.22184

Key words: *metamaterials; microstrip line; finite-difference time-domain (FDTD) method; split-ring resonators; retrieval method*

1. INTRODUCTION

Since their theoretical prediction by Veselago [1] and the experimental verification [2], left-handed materials (LHMS) have attracted much attention because of their novel properties such as negative permittivity and permeability. Various structural configurations for negative permittivity and permeability have been proposed, and especially split-ring resonators (SRRs) have been used to generate negative permeability within a frequency band [3].

Planar LHMs structures were introduced in Refs. 4 and 5. Both works demonstrated the backward wave phenomenon on an LHM transmission line that is composed of series capacitors and shunt inductors with normal nondispersive dielectric material substrate. For these types of structures, the propagation constant was derived and the dispersion curve was also shown in Ref. 6. These planar configurations for LH transmission have been applied to band pass filters and scanning antennas with guided and radiated waves, respectively, whereas a microstrip line with right-handed material substrate presents just a low pass filter characteristic.

The behavioral effect of dielectric SRRs on the transmitted signal of a microstrip line, with the ground plane modified by the inclusion of the SRRs, resulted in a band-stop filter in the microwave regime [7]. Also, a band pass filter for a coplanar waveguide structure was realized by using the bi-layer SRRs for negative effective permeability and wires for negative effective permittiviy [8]. The former works [4, 5] used conductor line patterns to obtain a backward wave property, and ring structures on the surface of normal dielectric substrate [7, 8] were utilized to realize filters. On the other hand, a rectangular SRR, which was proposed [9] at infrared frequencies and redesigned for microwave frequencies, [10] was implemented into a dielectric substrate for microwave filter [11]. We use this structure in this work. The axis of rectangular SRRs is aligned in the magnetic field direction so that they are excited by magnetic field and the permeability in this direction becomes Lorentz type. Thus, we embed dispersive and negative permeability properties that were previously in the microstrip design [7, 8] directly into the substrate, which relieves the design constraints on the printed lines and yields more degrees of freedom in the design.

In this article, by applying the image theory [12], one ring structure, instead of two rings, is proposed for lower insertion loss property. Here, because of the normal ground with directly embedded rings, we can use the image theory unlike the etched SRRs configuration [7]. The novel structure simplifies the fabrication and enables us to reduce the device volume of the substrate by 50%. The simulation and experimental results demonstrate that this method reduces loss out of stop band with enhanced filter property. SRRs are constructed in a dielectric substrate.

In this article, we show by using CST microwave studio (MWS) [13] and the retrieval method [14] that the proposed substrate has dispersive and negative permeability, which comes from the SRRs implanted into the substrate. The transmission properties of the device are found by the finite-difference time-domain (FDTD) method with the retrieved effective permeability, CST-MWS simulation and experimental results. The combination of the FDTD [15, 16] and retrieval method, which provides an efficient full-wave simulation tool for the SRRs configuration, is proposed to find the *S*-parameters, and transmission characteristic of a microstrip device, which uses a substrate embedded with ring structures inside. The ground and microstrip line on this substrate acts as a band-stop filter.

2. SUBSTRATE STRUCTURE WITH RINGS

The proposed device configuration is shown in Figure 1. A substrate is composed of many thin dielectric cards, which are stacked in the *x*-direction as shown in Figure 1(a). The lateral (*x*-direction)

periodicity is maintained by one dielectric card with SRRs metal patterns and three additional dielectric cards without SRRs metal patterns with all the cards placed adjacently. The dielectric card thicknesses in the x-direction are $t_1 = 0.5$ mm (cards with rings) and $t_2 = 1.1/3$ mm (cards without rings). The device length in the y-direction is 80 mm, and the relative permittivity of the dielectric material is four. The substrate thickness is 5 mm, and the total substrate width and the stripline width are 46 and 1.5 mm, respectively. The SRR ring design is shown in Figure 1(b). The distance between the rings in the x- and y-directions are 1.6 and 1.88 mm, respectively. Thus, the total number of a ring pair implemented into the substrate is 464 (16 in the y-direction and 29 in the x-direction).

The component of an incident wave for the proposed device has a z-directed electric field and an x-directed magnetic field. If a time-varying magnetic field has a component parallel to the axis, which penetrates into the SRR, a current flow is generated on the rings by the electromotive force. Thus, the ring structures are arranged for the rings to respond to the magnetic field as shown in Figure 1, and from the array of the SRR, it is expected that the permeability of the substrate may be approximated by a uniaxial tensor with two constant components and one dispersive component, which is known to have the Lorentz type dispersive behavior [2].

The two simulations used in this article are a 3D-FDTD with a retrieval method [14] and CST-MWS. For the 3D-FDTD calculation, Figure 2 shows the cross section at the input port (gray part

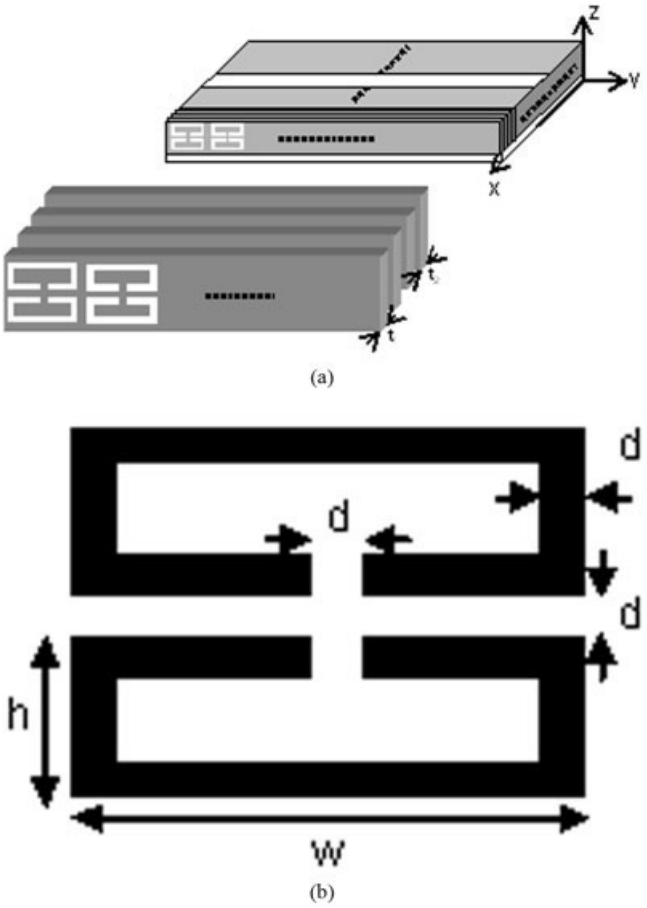

Figure 1 (a) Microstrip line structure with SRR configuration. (b) The design parameter values of SRR are: $w = 3.12$ mm, $h = 1.56$ mm, and $d = 0.24$ mm

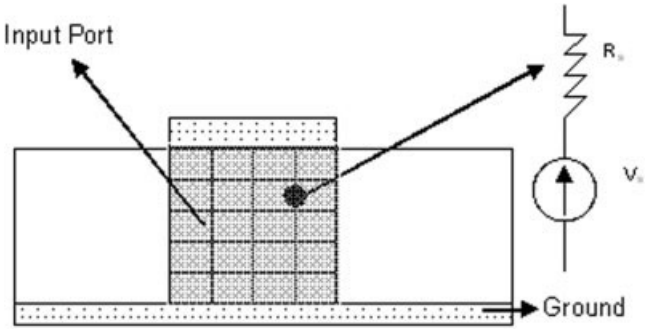

Figure 2 Cross sectional view of the microstrip line. The mesh lines are shown only under the stripline for the input port. E_z at input port is calculated by using R_s and V_s in FDTD code

between ground and signal line), and it is set at the rectangular surface between the ground and the stripline. A resistive voltage source for each cell at the input port is placed with the assumption of a z-directed lumped resistor element. Thus, E_z at the input port is given by [17].

$$E_z^{n+1/2} = \left(\frac{1 - \dfrac{\Delta t \Delta z}{2R_s\varepsilon_0\Delta x\Delta y}}{1 + \dfrac{\Delta t \Delta z}{2R_s\varepsilon_0\Delta x\Delta y}}\right)E_z^{n-1/2} + \left(\frac{\dfrac{\Delta t}{\varepsilon_0}}{1 + \dfrac{\Delta t \Delta z}{2R_s\varepsilon_0\Delta x\Delta y}}\right)\nabla \times \overline{H}^n + \left(\frac{\dfrac{\Delta t}{R_s\varepsilon_0\Delta x\Delta y}}{1 + \dfrac{\Delta t \Delta z}{2R_s\varepsilon_0\Delta x\Delta y}}\right)V_s^n \quad (1)$$

Here, Δx, Δy, Δz are the grid size in x, y, z-axis, respectively, and Δt is the time interval used in the FDTD computation. The parameters used for the FDTD simulations are cell sizes $\Delta x = 0.2$ mm, $\Delta y = 0.727$ mm, $\Delta z = 0.5$ mm, and $\Delta t = 0.717$ ps, which satisfies the Courant stability condition. The numbers of grid cells are 240, 130, and 30 in the x, y, and z-axis, respectively.

The input port is modeled by using the series connection of the voltage source and resistor, which represents the characteristic impedance of the coaxial cable. R_s (=50 Ω) is the internal source resistance, V_s is the source voltage, and ε_0 is the permittivity in the free space. Also, at the output port, a load resistor is considered to be 50 Ω by E_z [17].

This article uses the piecewise linear recursive convolution (PLRC) method to embed the dispersive medium property into the FDTD simulation [15] for the substrate of the Lorentz type. The extension of the formulation for the magnetic field results in

$$\overline{H}^{n+1} = \frac{\mu_\infty - \xi^0}{\mu_\infty + \chi^0 - \xi^0}\overline{H}^n - \frac{\Delta t}{\mu_0(\mu_\infty + \chi^0 - \xi^0)}\nabla \times \overline{E}^{n+1/2} + \frac{1}{\mu_\infty + \chi^0 - \xi^0}\psi^n \quad (2)$$

where μ_∞ is the permeability at infinite frequency, χ^0 and ξ^0 are the parameters defined in [16]:

$$\psi^n = \sum_{m=0}^{n-1}\{\overline{H}^{n-m}\Delta\chi^m + (\overline{H}^{n-m-1} - \overline{H}^{n-m})\Delta\xi^m\}. \quad (3)$$

By applying the outlined procedure of Ref. 18, the recursion relation is given by, for magnetic field,

$$^{\square}\psi^n = (\Delta\, ^{\square}\chi^0 - \Delta\hat{\xi}^0)\, H^n + \Delta\hat{\xi}^0 H^{n-1} + e^{(-\alpha+j\beta)\Delta t}\, ^{\square}\psi^{n-1} \quad (4)$$

where $\psi^n = Re\{^{\square}\psi^n\}$ which is called recursive accumulator for the Lorentz medium. From Eqs. (2) and (3) this method requires only one additional backstore variable per dispersive cell, and the calculation is performed without the cost of additional data storage.

3. SIMULATION AND MEASUREMENT RESULTS

For the described device structure, a PLRC FDTD, the MWS, and experimental results are given and compared. The numerical calculation process by the PLRC FDTD with the retrieval method is as follows. First, a unit ring configuration is simulated by the MWS to get *S*-parameters, transmission property of the material, and then they are applied into the retrieval method to determine the f_{mo} (resonant frequency) and f_{mp} (plasma frequency). Finally, these two frequency parameters are used in the PLRC FDTD full wave simulation. Figure 3 presents the real part of the relative permeability from calculation of the retrieval algorithm. The magnetic resonance from the ring structure is confirmed, and the plot has a shape similar to the Lorentz dispersive model [19]. Therefore, negative permeability is available in a frequency band between f_{mo} and f_{mp}. The calculated f_{mo} and f_{mp} are 6.58 and 7.6 GHz, respectively. It is also assumed that we have infinity-frequency permeability, $\mu_\infty = 1$, and the Lorentz model leads to zero-frequency permeability, $\mu_s = (f_{mp}/f_{mo})^2$. The thick curve indicates the S_{21} by the PLRC FDTD and the data from the retrieval method. The spike around 9 GHz in Figure 3 is because of the noise contained in the *S*-parameters, for which a sensitivity analysis can be found in Ref. 13.

Generally, LHM includes ring or rod structures, which are very small compared with the operating wavelength, and therefore significant memory is required to consider the detailed structure in FDTD simulations. However, this method is very useful because of the reduced memory size for calculation, because it does not consider the detailed configurations of the rings.

The dashed line in Figure 4 represents the transmission line characteristic simulated by the MWS. The full geometry of the

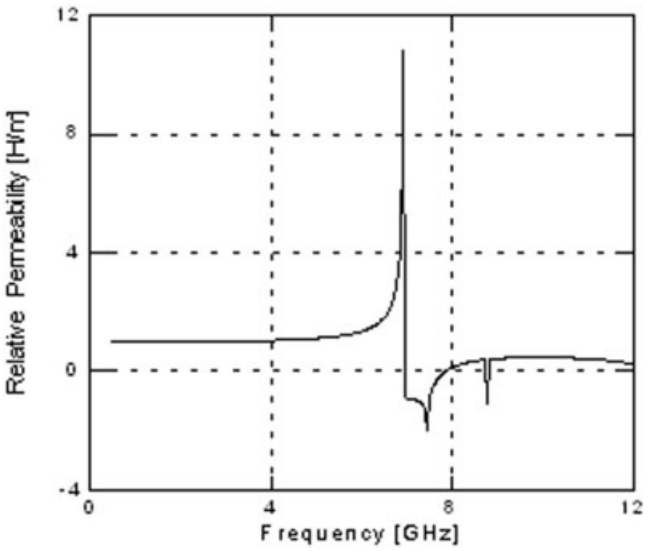

Figure 3 Real part of relative permeability

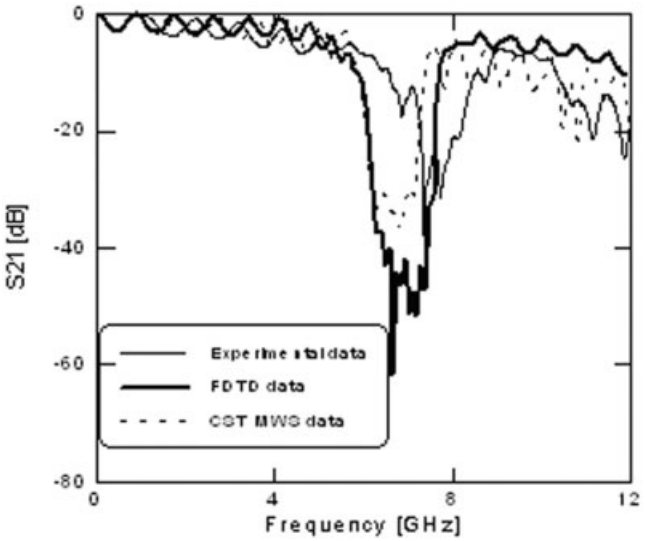

Figure 4 Transmission property of the device

device, which is described in the earlier section, was implemented in the software and simulated. All the rings, ground, and microstrip line are assumed to be perfect conductors both in the MWS and FDTD simulations. The metal thickness used in the simulations is assumed to be 0.035 mm. In the MWS tool, for mesh property for simulation, 'lines per wavelength' from the 'mesh' menu was set to 30 for 20 GHz. The data in Figure 4 present stop band property of the device. The center frequency of the stop band by the simulations is around 7 GHz, and the experimental one is about 7.8 GHz.

A vector network analyzer is used for the measurement of transmission property. SMA adapters are connected to the ends of the transmission line and connected to the ground plane and microstrip line. To test the homogeneity of the dispersive substrate, measurements are taken for three different placements of the microstrip. Some of insertion loss in Figure 4 is because of the radiation loss from the thick substrate.

The experimental result in Figure 4 has some discrepancy from the FDTD and CST MWS simulation data. The relative permittivity was set to four in both simulations, and this value was provided by the dielectric maker. However, the effective value of the relative permittivity should be less than four, because the substrate is composed of many dielectric cards, which leads to small air gaps between the cards because of the metal thickness. The air gap and ring patterns on the dielectric cards have relative permittivity value of 1.0 approximately. As mentioned earlier, one periodicity of the dielectric cards are composed of one 0.5-mm thick card and three 1.1/3-mm thick cards. Thus, a rough approximation ($4.0 \times 1565/1600 + 1.0 \times 35/1600$) results in 3.934 of relative permittivity.

Table 1 shows the CST MWS simulation data, with consideration of the lowered effective relative permittivity and mesh size ('lines per wavelength' in the 'mesh properties' option from the 'mesh' menu in the CST MWS). The simulations were carried out for a unit ring pair shown in Figure 1(b). First, the result in Table 1 depicts the effect of the frequency band shift because of the change of the effective relative permittivity of the substrate. The substrate with lower ε_r gives higher stop band. We can explain that this property from the relative permittivity which was calculated approximately above is one of the reasons of difference between the simulation and the experiment in Figure 4. Secondly, because

TABLE 1 The Center Frequency of the Stop Band According to the Relative Permittivity of the Substrate and the Lines per Wavelength

	Lines/λ			
ϵ_r	30	40	50	60
3.7	7.64	7.77	7.97	8.02
3.8	7.54	7.66	7.86	7.92
3.9	7.44	7.57	7.75	7.80
4.0	7.34	7.48	7.69	7.74

The lines per wavelength is a simulation input option of the CST MWS, and the maximum frequency for the simulation is 20 GHz. The unit for the center frequency is GHz here. This is a simulation result of a unit ring-pair structure by the CST MWS.

the thickness and dimension of the conductive rings are very thin in comparison with the wavelength at maximum simulation frequency (20 GHz in this article), we have saturated result with very small mesh size, 'lines per wavelength' of 60 or greater value. From the results with relative permittivity of 3.9, a stop band frequency is expected to be between 7.74 and 7.80 GHz, which is very close to the experiment data in Figure 4. But this setup in the CST MWS requires too much of memory resource to run a simulation on a PC for the device shown in Figure 1(a). Thus, from the discussion above, the frequency shift between experiment and simulation results in Figure 4 comes from the permittivity difference and mesh size. The significant losses at high frequency observed in Figure 4 result from radiation because of the large thickness of the substrate. To reduce the loss, a half SRR substrate is proposed. As shown in Figure 1(a), the SRR is composed of two rings which are symmetric in that they are mirror images of each other across a line parallel to the *y*-axis. Figure 5 shows the current density from the MWS simulation on the rings at 7.34 GHz where relative permeability has negative value. Figure 5(a) corresponds to the case of maximum H_x and Figure 5(b) is at the phase after 180 degree. A current flow on the rings is induced either by H_x or $-H_x$, and the upper and lower rings have the opposite and same direction in the *y*- and *z*-directions, respectively. Thus, we can use only the upper part of the ring pairs by applying the image theory as shown in Figure 6. A dielectric card with half thickness is shown and ground is placed at the bottom of many dielectric cards. Figure 7 exhibits improved filter characteristic with half thickness substrate (2.5 mm). The dotted line (CST MWS data in Fig. 4) is plotted again for comparison. In the frequency range above stop band, the full geometry simulation by the CST MWS presents an improvement of loss by about 5–8 dB.

In Figure 7, the experimental result of center frequency has some discrepancy from the simulation. It results from a small gap d_2 in Figure 6. For an ideal case, d_1 in Figure 6 is $d/2 = 0.12$ mm and d_2 is zero. However, in the experiment, we came to have a little air gap between the ground plane and the dielectric cards, while we stacked the cards manually in the *x*-direction, preparing for measurement. The simulation results in Table 2 show the effect of the gap d_2. Half ring structure with a ground plane was simulated by the CST MWS. The relative permittivity of the substrate was set to 3.94. From the result in Table 2, we can deduce that the effective air gap should be around 50–60 μm for the experimental data in Figure 7. According to Ref. 2, theoretically both f_{mo} and f_{mp} are proportional to $1/\sqrt{C}$, where C is the capacitance per unit area. Thus, the stop band is shifted to a higher range as expected, because the air gap decreases the value of C.

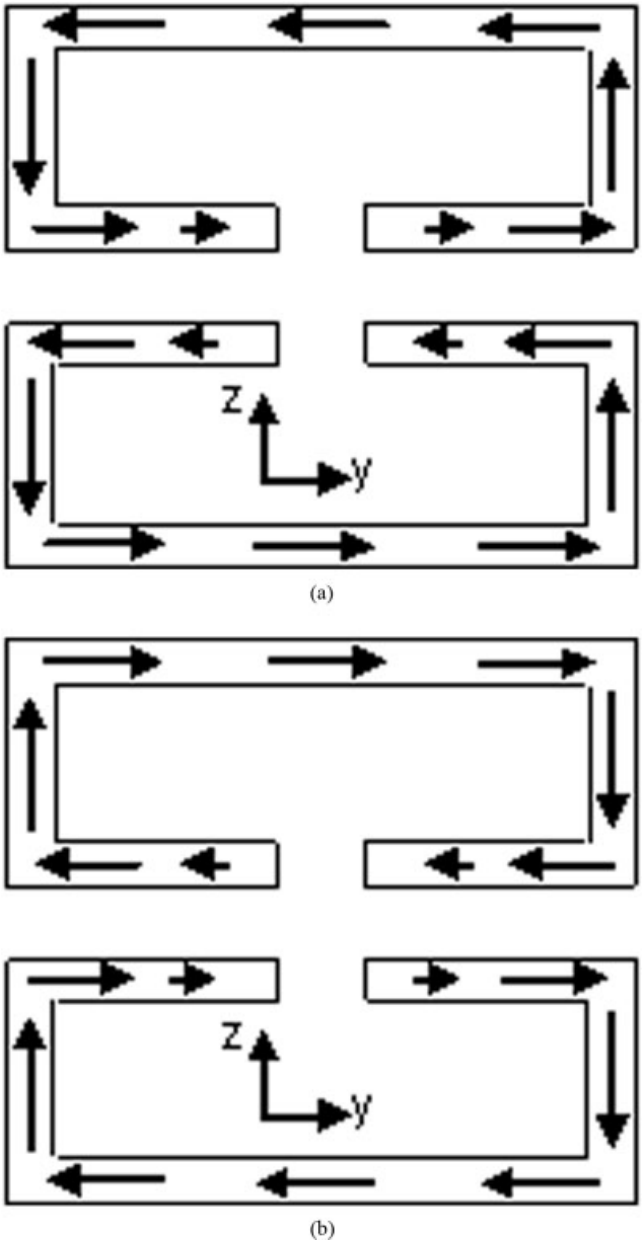

Figure 5 Current density on a unit ring pair at 7.34 GHz with (a) maximum value of H_x inside the rings and (b) minimum value of H_x inside the rings

4. CONCLUSION

We have proposed a microstrip line on a substrate which has ring structures and effectively presents a dispersive and negative permeability component in one direction spatially. For the analysis of metamaterial device, a dispersive FDTD method combined with the retrieval method has been proposed and applied. This method

Figure 6 A dielectric card for the substrate with upper part of the rings. The image is also shown

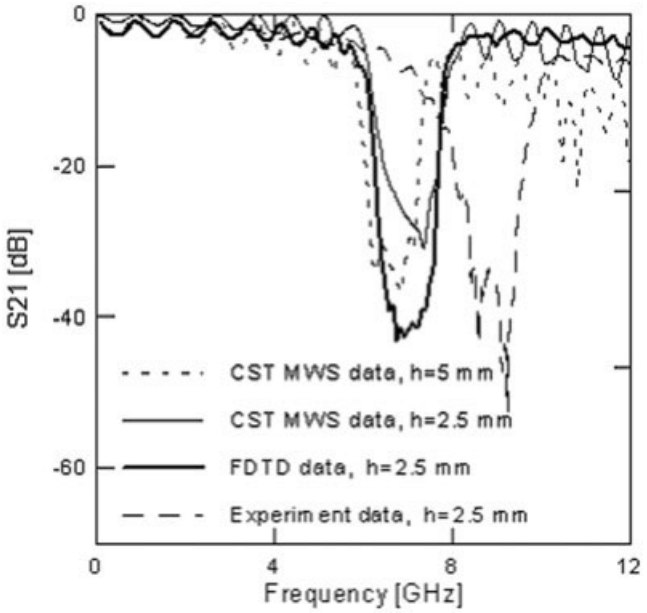

Figure 7 S_{21} data comparison with the substrates, including, ring pairs and upper part of the rings

has the advantage of reducing memory size comparatively, because the full-wave simulation considering the SRRs structure for exact results requires too much memory. The numerical simulation and experimental results have shown stop-band phenomenon of the device between the resonance and the plasma frequency. Also, the radiation loss was reduced by applying the image theory and using thin substrate.

The bandwidth and operational center frequency can be controlled by tuning the resonant and plasma frequency from the design of the SRRs. This kind of substrate embedded with SRRs is expected to be used for other microwave devices and applications.

ACKNOWLEDGMENT

This work was supported by the Korea Research Foundation Grant funded by the Korea Government (MOEHRD, Basic Research Promotion Fund) (M01–2004-000–10187–0). This material is based upon the work supported under a National Science Foundation Graduate Research Fellowship. This work was sponsored by the Department of the Air Force under Air Force Contract F19628–00-C-0002, and the ONR under Contract N00014–01-1–0713. Opinions, interpretations, conclusions, and recommendations are those of the author and are not necessarily endorsed by the United States Government.

TABLE 2 The Center Frequency of the Stop Band According to the Lines per Wavelength and the Gap Between Ground Plane and the Substrate (d_2)

	d_2 (μm)			
Lines/λ	30	40	50	60
30	7.85	7.92	7.98	8.70
60	8.50	8.67	8.79	8.90

The unit for the center frequency is GHz here. This is a simulation result of a half ring structure by the CST MWS. ϵ_r of the substrate for the simulation was set to 3.94.

REFERENCES

1. V.G. Veselago, The electrodynamics of substances with simultaneously negative values of ε and μ, Sov Phys Usp 10 (1968), 509–514.
2. D.R. Smith, W.J. Padilla, D.C. Vier, S.C. Nemat-Nasser, and S. Schultz, Composite medium with simultaneously negative permeability and permittivity, Phys Rev Lett 84 (2000), 4184–4187.
3. J.B. Pendry, A.J. Holden, D.J. Robbins, and W.J. Stewart, Magnetism from conductors and enhanced nonlinear phenomena, IEEE Trans Microwave Theory Tech 47 (1999), 2075–2084.
4. L. Liu, C. Caloz, and T. Itoh, Dominant mode leaky wave antenna with backfire-to-endfire scanning capability, Electron Lett 38 (2002), 1414–1416.
5. A. Grbic and G.V. Eleftheriades, Experimental verification of backward wave radiation from a negative refractive index metamaterial, J Appl Phys 92 (2002), 5930–5935.
6. C. Caloz and T. Itoh, Transmission line approach of left-handed materials and microstrip implementation of an artificial lh transmission line, IEEE Trans Antennas Propag 52 (2004), 1159–1166.
7. S.N. Burokur, M. Latrach, and S. Toutain, Study of the effect of dielectric split-ring resonators on microstrip-line transmission, Microwave Opt Technol Lett 44 (2005), 445–448.
8. F. Falcone, F. Martin, J. Bonache, R. Marques, T. Lopetegi, and M. Sorolla, Left handed coplanar waveguide band pass filters based on bi-layer split ring resonators, IEEE Microwave Wireless Compon Lett 14 (2004), 10–12.
9. S. O'Brien and J.B. Pendry, Magnetic activity at infrared frequencies in structured metallic photonic crystals, J Phys: Condens Matter 14 (2002), 6383–6394.
10. T.M. Grzegorczyk, C.D. Moss, J. Lu, X. Chen, J. Pacheco, Jr., and J.A. Kong, Properties of left-handed metamaterials: Transmission, backward phase, negative refraction, focusing, IEEE Trans Microwave Theory Tech 53 (2005), 2956–2967.
11. Z.M. Thomas, T.M. Grzegorczyk, B.-I. Wu, and J.A. Kong, Enhanced microstrip stopband filter using a left-handed metamaterial substrate, Microwave Opt Technol Lett, in press.
12. J.A. Kong, Electromagnetic wave theory, EMW, New York, 2000.
13. CST Microwave studio, Version 5.0.2., 2004.
14. X. Chen, T.M. Grzegorczyk, B.-I. Wu, J. Pacheco, and J.A. Kong, Robust method to retrieve the constitutive effective parameters of metamaterials, Phy Rev E 70 (2004), 016608.
15. K.S. Yee, Numerical solution of initial boundary value problems involving Maxwell's equations in isotropic media, IEEE Trans Antennas Propag 14 (1966), 302–307.
16. D.F. Kelley and R.J. Luebbers, Piecewise linear recursive convolution for dispersive media using FDTD, IEEE Trans Antennas Propag 44 (1996), 792–797.
17. M. Piket-May, A. Taflove, and J. Baron, FD-TD modeling of digital signal propagation in 3-D circuits with passive and active loads, IEEE Trans Microwave Theory Tech 42 (1994), 1524–1523.
18. R.J. Luebbers, F.P. Hunsberger, K.S. Kunz, R.B, Standler, and M. Schneider, A frequency-dependent finite-difference time-domain formulation for dispersive materials, IEEE Trans Electromagn Compat 32 (1990), 222–227.
19. R.A. Shelby, D.R. Smith, and S. Schultz, Experimental verification of a negative index of refraction, Science 292 (2001), 77–79.